HELDA
HELSINGIN YLIOPISTO
HELSINGFORS UNIVERSITET
UNIVERSITY OF HELSINKI

UNIVERSITY OF HELSINKI

https://helda.helsinki.fi

Surface air relative humidities spuriously exceeding 100% in CMIP5 model output and their impact on future projections

Ruosteenoja, Kimmo

2017-09-27

Ruosteenoja , K , Jylha , K , Räisänen , J & Mäkelä , A 2017 , ' Surface air relative humidities spuriously exceeding 100% in CMIP5 model output and their impact on future projections ' , Journal of Geophysical Research : Atmospheres , vol. 122 , no. 18 , pp. 9557-9568 . https://doi.org/10.1002/2017JD026909

http://hdl.handle.net/10138/308149
https://doi.org/10.1002/2017JD026909

cc_by_nc_sa
publishedVersion

Downloaded from Helda, University of Helsinki institutional repository.

This is an electronic reprint of the original article.

This reprint may differ from the original in pagination and typographic detail.

Please cite the original version.

AGU PUBLICATIONS

JGR

Journal of Geophysical Research: Atmospheres

RESEARCH ARTICLE
10.1002/2017JD026909

Key Points:
- Near-surface air relative humidities considerably above 100% are common in high latitudes in the output of CMIP5 climate models
- The severity of supersaturations varies much between the models, and three candidate explanations for the issue are given
- Projected future warming acts to reduce supersaturation, inducing a spurious negative trend in humidity for wide high-latitude areas

Supporting Information:
- Supporting Information S1

Correspondence to:
K. Ruosteenoja,
kimmo.ruosteenoja@fmi.fi

Citation:
Ruosteenoja K., K. Jylhä, J. Räisänen, and A. Mäkelä (2017), Surface air relative humidities spuriously exceeding 100% in CMIP5 model output and their impact on future projections, *J. Geophys. Res. Atmos.*, *122*, 9557–9568, doi:10.1002/2017JD026909.

Received 4 APR 2017
Accepted 19 AUG 2017
Accepted article online 24 AUG 2017
Published online 18 SEP 2017

©2017. American Geophysical Union. All Rights Reserved.

Surface air relative humidities spuriously exceeding 100% in CMIP5 model output and their impact on future projections

Kimmo Ruosteenoja[1], Kirsti Jylhä[1], Jouni Räisänen[2], and Antti Mäkelä[1]

[1]Finnish Meteorological Institute, Helsinki, Finland, [2]Department of Physics, University of Helsinki, Helsinki, Finland

Abstract In 17 out of the 29 Phase 5 of Coupled Model Intercomparison Project (CMIP5) climate models examined in this work, near-surface air relative humidity (RH) frequently exceeded 100% with respect to ice in polar areas in winter. The degree of supersaturation varied considerably across the models, and the same evidently applies to the causes of the phenomenon. Consultations with the modeling groups revealed three categories of explanations for supersaturation occurrence: specification of RH with respect to ice rather than liquid water; inconsistencies in the determination of specific humidity and air temperature for the near-surface level; and the nonlinearity of saturated specific humidity as a function of temperature. Modeled global warming tended to reduce the artificial supersaturations, inducing a spurious negative trend in the future RH change. For example, over East Antarctica under Representative Concentration Pathway 8.5, the multimodel mean RH would decrease by about 10% by the end of the ongoing century. Truncation of overly high RHs to a maximum value of 100% cut the RH response close to zero. In Siberia and northern North America, truncation even reversed the sign of the response. The institutes responsible for the CMIP6 model experiments should be aware of the supersaturation issue, and the algorithms used to produce near-surface RH should be developed to eliminate the problem before publishing the RH output data.

Plain Language Summary In the atmosphere, observed relative humidity is between 0% and 100%. However, some climate models produce spurious higher than 100% humidities. The problem only concerns polar areas in winter. As temperatures rise in the future, such model-produced excessively high relative humidities partially vanish. Unfortunately, this induces a spurious negative trend in the future humidity projections. Such a spurious component in the simulated trend complicates discerning the real physically based trend. The spurious trend could be eliminated by truncating the portion of relative humidity that exceeds 100% in the model output data. Even so, this may not be fully adequate for elaborating reliable humidity projections for polar areas. Therefore, it is highly desirable that the relative humidity calculations in the climate models would be developed so that unrealistic relative humidities would not occur in future model generations. We emphasize that this issue only concerns humidity projections and does not affect model-based predictions of temperature and precipitation change.

1. Introduction

In tandem with global warming, near-surface relative humidity (RH) is projected to decrease in a majority of continental areas [*Intergovernmental Panel on Climate Change (IPCC)*, 2013]. According to *Berg et al.* [2016] and *Byrne and O'Gorman* [2016], this is basically caused by more rapid warming over continents compared with oceans. Consequently, in the air advected from oceans to continents, specific humidity increases more slowly than the saturation specific humidity over the continents. An additional factor reducing RH over the continents is the feedback induced by diminishing soil moisture.

In general, models simulate a decrease in RH for polar areas in winter as well, even though the intermodel agreement is fairly modest [*IPCC*, 2013, Figure 12.21]. On the other hand, simulated changes in several other climate variables rather exhibit a tendency toward wetter conditions: winter precipitation and cloudiness are simulated to increase at high latitudes, for instance [e.g., *IPCC*, 2013, Figures 12.22 and 12.17]. Moreover, in their study based on a limited ensemble of previous generation climate models, *Ruosteenoja and Räisänen* [2013] reported an increase in wintertime 1000 hPa RH for northern Europe. In northern boreal areas

during the past few decades, observational analyses likewise show an overall moistening trend in RH [*Willett et al.*, 2014].

In the present work, founded on recent-generation global climate models (GCMs) participating in the Phase 5 of Coupled Model Intercomparison Project (CMIP5), we demonstrate that humidities distinctly above 100% with respect to ice are very common in the archived model output files. Supersaturations cluster in the high-latitude areas of the winter hemisphere. The main purpose of the work is to explore how this artifact influences the future projections of RH, but potential explanations for the supersaturation phenomenon are sought as well. The occurrence of supersaturation in model output was mentioned in *Lehtonen et al.* [2016], but to our knowledge, the issue has not been investigated in detail hitherto.

The water vapor capacity of air is largest in high temperatures, and accordingly, the impacts of RH have been studied most widely in warm conditions. To mention some examples, RH contributes to the growth of crops [e.g., *Asseng et al.*, 2015], human comfort and heat stress [e.g., *Willett and Sherwood*, 2012; *Knutson and Ploshay*, 2016], wildfires [e.g., *Lehtonen et al.*, 2014; *Vajda et al.*, 2014], and surface evapotranspiration and soil moisture [e.g., *Seneviratne et al.*, 2010; *Ruosteenoja et al.*, 2017]. Even so, air humidity has multiple implications in areas with cold climate as well. Humidity deficit in the air, in conjunction with katabatic winds, acts to evaporate ice in the Antarctic ice sheet, thus being one determinant for the surface mass balance [*van den Broeke et al.*, 2006; *Andersen et al.*, 2015]. Accumulation of ice and snow in wind power mills [*Parent and Ilinca*, 2011], electric wires [*Makkonen and Wichura*, 2010], and tree crowns in boreal forests [*Lehtonen et al.*, 2016] is affected by air humidity. High RH exacerbates moisture loads in buildings, increasing the risks of mold exposure in the structures [*Viitanen et al.*, 2010] and frost damages in concrete facades [*Lahdensivu et al.*, 2011]. Furthermore, RH is a key factor for the formation of fog [e.g., *Ding and Liu*, 2014] and cloudiness [e.g., *Andreas et al.*, 2002], with implications on the radiative balance of the surface.

Although the detected supersaturations occur exclusively at high latitudes, this phenomenon may be an indication of more general deficiencies in model-produced near-surface humidities. In section 5.2, we present three viable explanations for the unrealistic values of RH at the near-surface level. These alternative explanations are based on correspondence with multiple modeling groups as well as on our own analyses. Two of these three potential causes would also have influence on RH output outside of polar areas.

In this paper, we first introduce the GCM data exploited (section 2). Thereafter, we explore the incidence of higher than 100% humidities in the GCM output (section 3) and assess the influence of supersaturation occurrence on the future projections of RH (section 4). This is performed by comparing RH projections derived from the unmodified GCM output to those calculated after truncating higher than 100% humidities in the output data. In order to discern the influence of the RH artifacts on the climate change signal most effectively, we focus on the high-emission Representative Concentration Pathway scenario RCP8.5. Next, we contemplate to what extent the high RHs occurring in the model output are realistic and explore potential causes for their occurrence (section 5). Finally, conclusions are presented in section 6.

2. Model Data

The climate models analyzed in this work are listed in Table 1. Monthly mean RH data were studied for 29 GCMs, considering all the parallel runs available. Daily mean data were examined only from 18 GCMs (Table 1). The number of GCMs was restricted by the fact that some modeling centers did not provide any RH data and several others have published RH only at monthly but not at daily time frequency. Moreover, for daily data, we did not include more than two model versions from any individual center and only analyzed a one parallel run for every GCM.

In the model output files, RH is expressed with respect to liquid water in above zero temperatures and to ice in below-freezing temperatures. To calculate multimodel statistics, RH data represented on the original grids of each individual model were interpolated linearly onto a common 2.5° latitude-longitude grid.

3. Occurrence of Supersaturation in Model Output

To assess the severity of the supersaturation issue in individual model runs, we calculated, separately for every calendar month and grid point of the 2.5° grid, a temporal mean for the exceedance of RH= 100%:

$$\mathrm{EX} = \frac{1}{y_2 - y_1 + 1} \sum_{y=y_1}^{y_2} \max(\mathrm{RH} - 100\%, 0) \tag{1}$$

Table 1. Global Climate Models Analyzed for the Occurrence of Supersaturated Near-Surface Relative Humidities[a]

Model	Country	N_{mon}	N_{day}	EX^N_{hist}	$EX^N_{RCP8.5}$	EX^S_{hist}	$EX^S_{RCP8.5}$
MIROC5	Japan	3	1	5.60	0.76	2.42	1.69
MIROC-ESM	Japan	1	1	0.00	0.00	0.00	0.00
MIROC-ESM-CHEM	Japan	1	-	0.00	0.00	0.00	0.00
MRI-CGCM3	Japan	1	1	0.00	0.00	0.00	0.00
BNU-ESM	China	1	1	0.00	0.00	0.00	0.00
FGOALS-s2	China	3	1	0.00	0.00	0.00	0.00
BCC-CSM1-1	China	1	1	0.00	0.00	0.00	0.00
INMCM4	Russia	1	1	2.81	1.54	19.61	13.71
NorESM1-M	Norway	1	1	0.40	0.02	0.90	0.39
NorESM1-ME	Norway	1	-	0.47	0.03	1.16	0.49
HadGEM2-ES	UK	4	1	0.94	0.21	3.88	2.32
HadGEM2-CC	UK	3	1	1.06	0.26	3.84	2.42
HadGEM2-AO	UK	1	-	0.86	0.32	3.76	2.13
CNRM-CM5	France	5	1	0.00	0.00	0.00	0.00
IPSL-CM5A-LR	France	4	1	0.00	0.00	0.00	0.00
IPSL-CM5A-MR	France	1	1	0.00	0.00	0.00	0.00
IPSL-CM5B-LR	France	1	-	0.00	0.00	0.00	0.00
GFDL-CM3	USA	1	1	0.66	0.21	6.93	4.08
GFDL-ESM2G	USA	1	-	0.38	0.24	1.39	1.09
GFDL-ESM2 M	USA	1	1	0.33	0.27	1.36	1.07
GISS-E2-R	USA	1	-	0.16	0.06	4.02	2.51
GISS-E2-H	USA	1	-	0.20	0.04	3.32	1.92
NCAR-CCSM4	USA	6	1	0.22	0.02	1.06	0.30
NCAR-CESM1-CAM5	USA	3	-	4.73	1.56	7.69	4.51
NCAR-CESM1-BGC	USA	1	-	0.21	0.02	1.01	0.31
CanESM2	Canada	5	1	0.00	0.00	0.00	0.00
ACCESS1-0	Australia	1	-	1.09	0.39	4.24	2.77
ACCESS1-3	Australia	1	-	3.05	1.35	5.86	4.37
CSIRO-Mk3-6-0	Australia	10	1	0.00	0.00	0.00	0.00

[a]The first and second columns state the model acronym and the country of origin. Third and fourth columns indicate the count of parallel runs included in the analysis of the monthly and daily model output for the RCP8.5 scenario. The last four columns show the spatially averaged temporal means for the 100% RH exceedances in northern areas from December to February (60–90°N; index *N*) and southern areas from June to August (60–90°S; index *S*); both are given separately for the periods 1961–2005 (EX_{hist}) and 2070–2099 under RCP8.5 ($EX_{RCP8.5}$) (unit percent).

where y_1 and y_2 stand for the first and last year of the period examined and RH is the modeled monthly mean humidity. To eliminate the influence of potential rounding errors, only cases with RH >100.1% were incorporated in the sum. Note that EX characterizes both the frequency and magnitude of the supersaturation events.

Humidities higher than 100% are concentrated in the polar areas of the winter hemisphere. Considering the multimodel mean (Figure 1), the temporally averaged supersaturation is largest over central East Antarctica in June–August; over wide areas, EX exceeds 20%. Less extreme but still notable supersaturation occurs in the ocean areas adjacent to Antarctica and in the polar areas of Northern Hemisphere. In summer, the supersaturations are far weaker than in winter, the maximum values of EX being ~1% in the south and ~0.1% in the north.

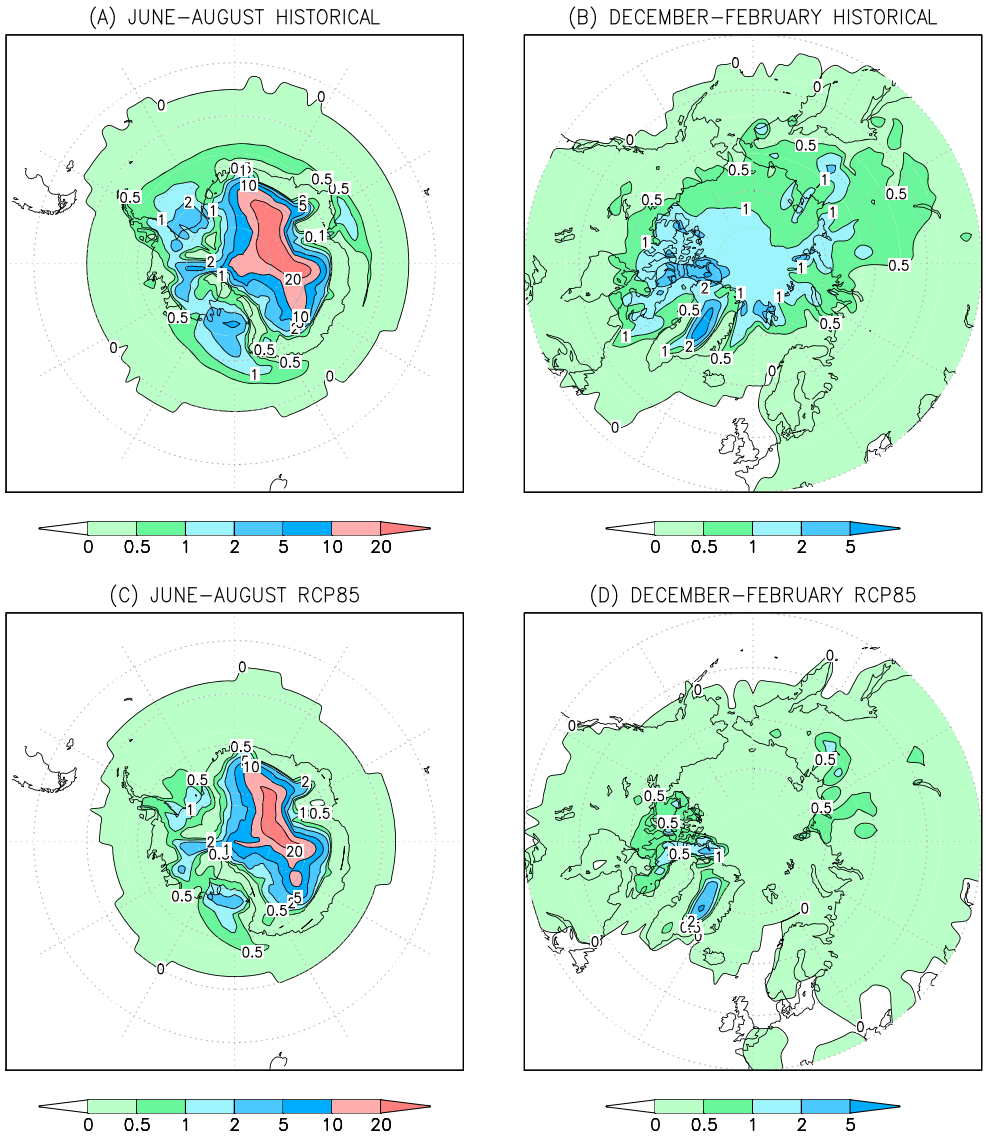

Figure 1. Temporally averaged supersaturation (in percent; see equation (1) in (a) southern and (b) northern polar areas in winter during the period 1961–2005; the mean over the 29 GCMs is listed in Table 1. (c and d) The corresponding distributions for the period 2070–2099 under RCP8.5.

The degree of supersaturation varies widely across the 29 GCMs. To elucidate this, a spatial average of the supersaturation parameter EX from the 60th latitude to the pole is shown in Table 1 for the individual GCMs, and the geographical distribution of EX for the four worst-behaving models in the corresponding hemisphere is given in Figures 2 and 3. The most severe supersaturation, with the spatially averaged EX higher than 5% in either polar area during the historical period 1961–2005, occurs in INMCM4, NCAR-CESM1-CAM5, GFDL-CM3, ACCESS1-3, and MIROC5. In the south, in all cases EX is largest over East Antarctica (Figure 2); in INMCM4 and GFDL-CM3, supersaturation exceeds 200%. In the north, in MIROC5 and NCAR-CESM1-CAM5 the occurrence of supersaturation is concentrated over the Arctic Ocean and its marginal seas while for ACCESS1-3 and INMCM4, continental areas are affected most seriously (Figure 3). On the other hand, in the monthly mean output files of 12 GCMs, RH never exceeds 100%.

When studying the temporal covariability of monthly mean RH and temperature, we found that the highest relative humidities typically coincided with negative temperature anomalies while mild months tended to show weaker supersaturation. Moreover, the simulated supersaturations are mitigated by the end of the

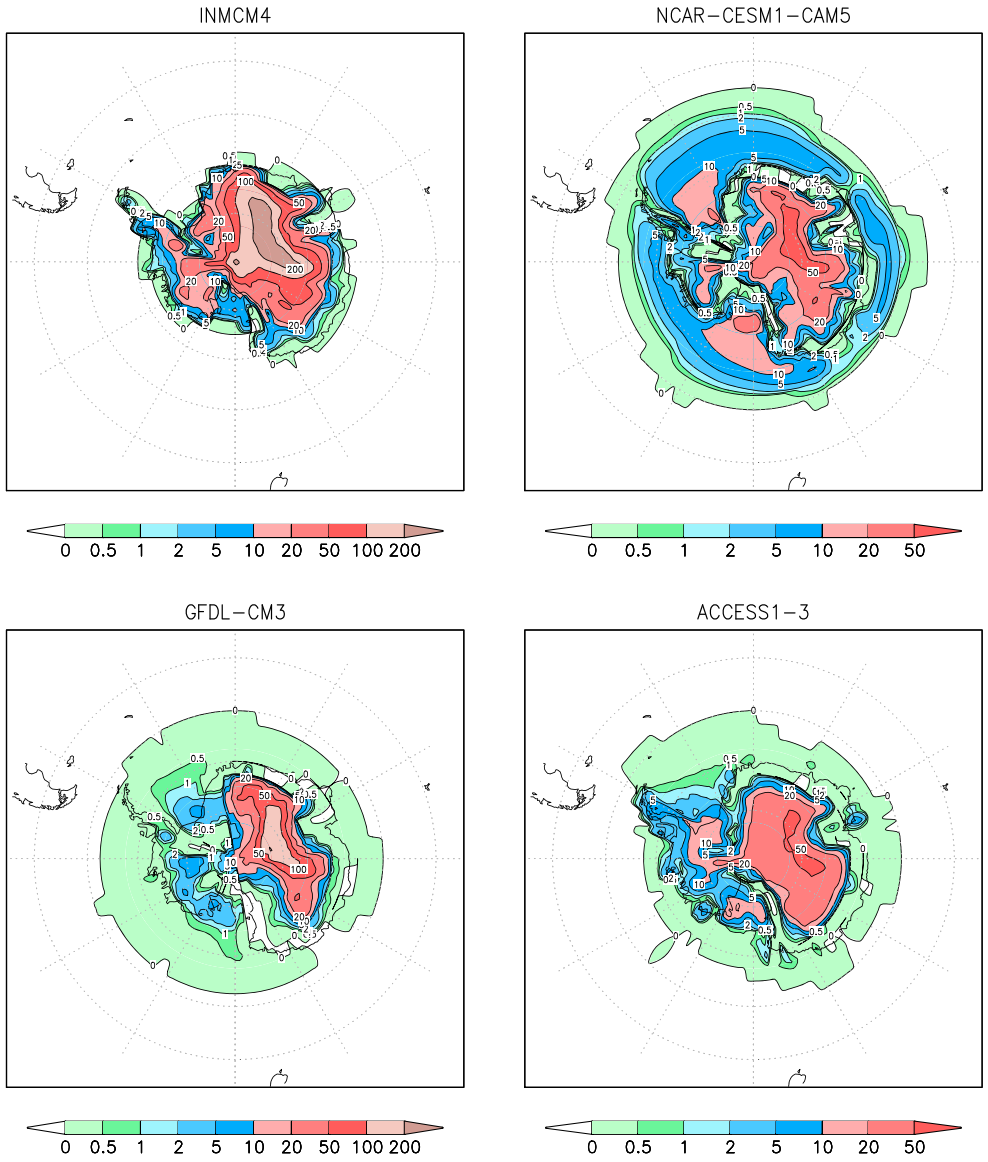

Figure 2. Temporally averaged supersaturation EX (in percent, see equation (1) for the southern winter months (June–August) during the period 1961–2005 derived from the historical runs of four GCMs: INMCM4, NCAR-CESM1-CAM5, GFDL-CM3, and ACCESS1-3. Note the quasi-logarithmic color scale.

21st century (Table 1 and Figure 1), along with the projected warming. For models showing the strongest supersaturation, the spatially averaged EX in southern winter is reduced by more than a fourth compared to the historical period values. For several other models with a more modest supersaturation, the decrease in relative terms is even larger. In northern polar areas, EX declines by more than a half, with the exception of three models. These findings suggest that the supersaturation problem is closely related to the occurrence of low temperatures.

In the output files of the most GCMs studied in this work, monthly mean RH equaled the linear average of the daily means. Thereby, supersaturation existed in the daily data of all those GCMs in which the supersaturation occurred in the monthly mean output (Table 1). In addition, higher than 100% humidities were found in the daily mean data of MIROC-ESM and FGOALS-s2, even though supersaturations were absent in the monthly means. A closer inspection of the MIROC-ESM output files revealed that in those months when the average calculated from the daily means exceeded 100%, in the monthly mean output file RH ≡ 100%; i.e., supersaturations have been truncated in the monthly but not in the daily mean data (in FGOALS-s2, monthly values were

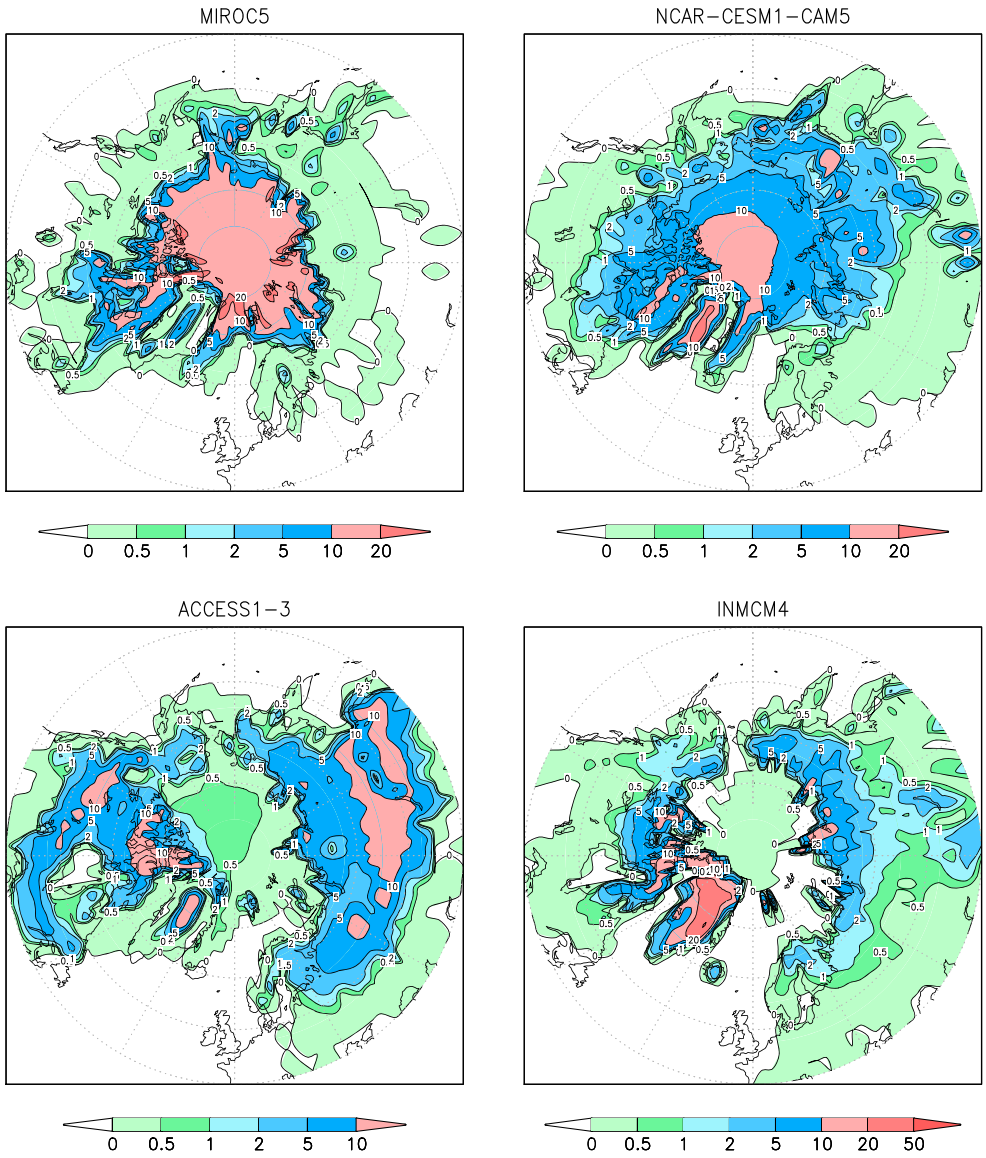

Figure 3. Temporally averaged supersaturation (in percent) for the northern winter months (December–February) during the period 1961–2005 derived from the historical runs of four GCMs: MIROC5, NCAR-CESM1-CAM5, ACCESS1-3, and INMCM4.

not the simple averages of daily means). Furthermore, in many GCMs in which exceedances occurred neither in the daily nor monthly data, humidities between 99.9 and 100% were very common in polar areas, having relative frequencies up to ~50%. This might indicate that, in these models as well, exceedances of 100% RH would have occurred in the original model output but they have been cleaned out before publishing the archived files.

Finally, it should be mentioned that in the output of two GCMs (INMCM4 and GFDL-ESM2M) negative relative humidities were encountered in small areas at high latitudes.

4. Influence of Modeled Supersaturation on Future RH Projections

To assess the importance of the simulated supersaturations on the future projections of RH change, the projections were calculated with three alternative methods. First, we used the original unmodified model output. Second, the projections were calculated after truncating all the supersaturated humidities to 100% in the monthly mean model output. Third, truncation to 100% was carried out for the daily data; the truncated daily

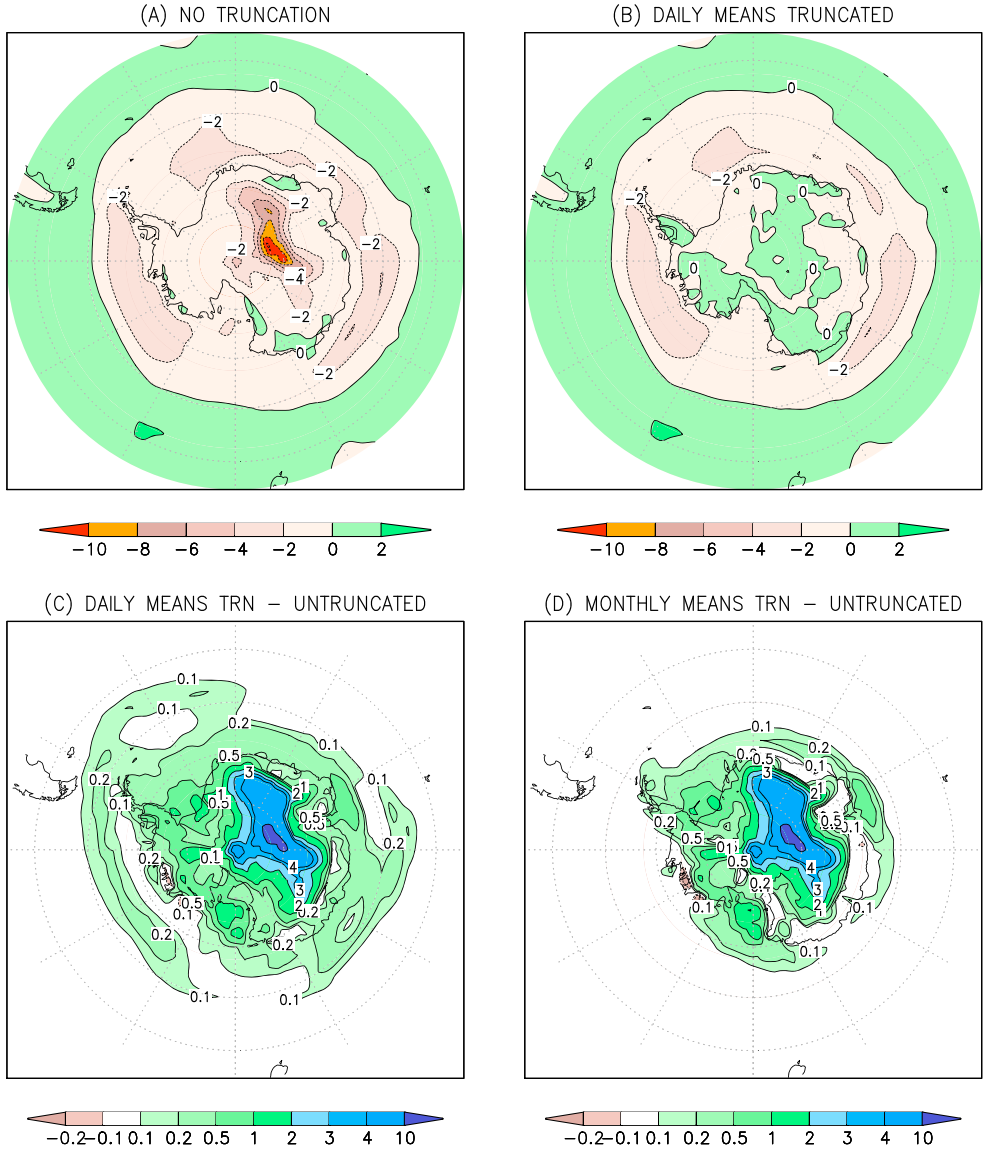

Figure 4. Projected changes in RH (in percent) in Southern Hemisphere winter (June–August) from 1981–2010 to 2070–2099 under RCP8.5 as the mean of the 18 GCM simulations listed in column 4 of Table 1: (a) the responses derived from the original model output and (b) from the output with relative humidities higher than 100% truncated in daily mean data; (c) the difference between Figures 4b and 4a and (d) the difference between the multimodel mean responses with supersaturations truncated from monthly means versus without truncation. For consistency, in creating these maps, only a single parallel run was included from every model.

means were then used to calculate monthly means, from which the actual future projections were derived. In all three alternatives, the projections were first calculated separately for every model, and the responses were then averaged over the 18-GCM ensemble by giving equal weights for all models.

The influence of truncation is most pronounced over Antarctica (Figure 4). When using the unmodified model output, RH would decrease virtually everywhere to the south of ~ 60°S, by up to 12% over the central East-Antarctic plateau (Figure 4a). When all the exceedances over RH=100% are truncated from daily data, the calculated RH response over the Antarctic continent is invariably close to zero and in wide areas even slightly positive (Figure 4b). Truncation makes the RH response more humid everywhere over the continent, with the largest impact (locally > 10%) over East Antarctica (Figure 4c). (Note that, in the models and areas suffering from severe supersaturation, the truncated RH equals 100% for a large portion of time, both during the baseline and future periods. This inevitably results in a small response in the time-mean RH for those models. This feature is to some extent reflected in the multimodel mean response as well.)

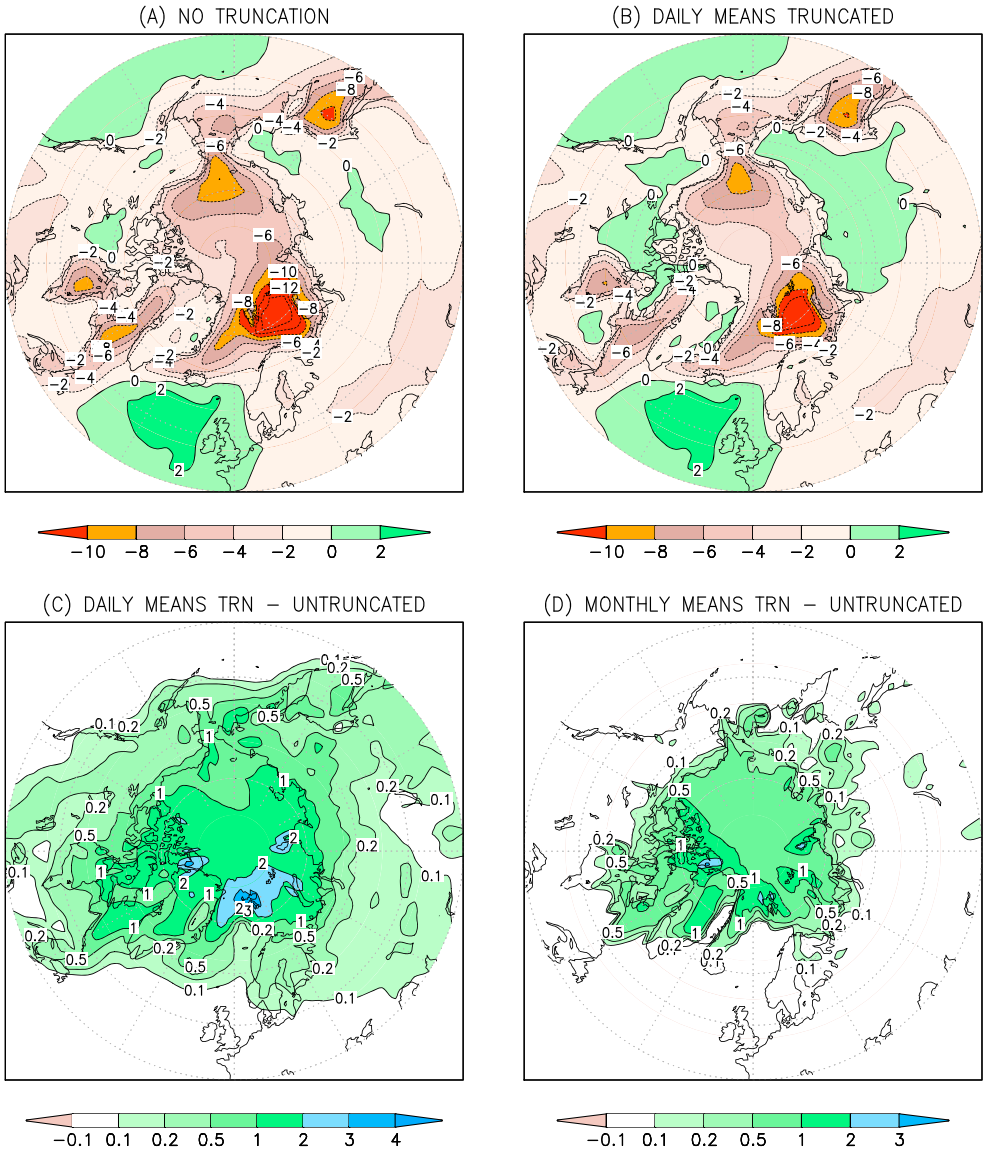

Figure 5. As in Figure 4 but for the Northern Hemisphere winter (December–February).

In northern polar areas, the influence of truncation is qualitatively similar but weaker than in the south (Figure 5). The truncated RH projections are typically 1–3% moister than those derived from the unmodified model output, with the largest deviations near Spitsbergen (Figure 5c). In wide areas of Siberia and northern North America, the sign of projected RH change reverses from negative to positive as a consequence of truncation (Figures 5a and 5b).

The impact of truncation is qualitatively similar regardless of whether supersaturations are cut off from the daily or monthly means (Figures 4c and 4d and 5c and 5d). Over the areas of moderate supersaturation, however, truncation works most effectively when implemented for the daily means; this is particularly evident in the north. When studying the monthly mean data, the influence of truncation is fairly similar regardless of whether all the 29 GCMs (Figures S1 and S2 in the supporting information) or only 18 GCMs (Figures 4 and 5) are studied.

Outside of the polar areas of the winter hemisphere, the influence of truncation was negligible (a few tenths of percent at maximum) or zero, regardless of the truncation method used.

The importance of truncating supersaturations varies strongly among the models, being largest for those GCMs that exhibit the most severe supersaturation during the baseline period (Table 1). In this respect,

the response of INMCM4 over southern polar areas constitutes an illustrative example (Figure S3). Without truncation, RH would (unphysically) decrease by up to more than 100% while the corresponding response calculated from data truncated at the daily level is smaller than 1%. In GFDL-CM3, truncation locally reduces drying by more than 50% and in NCAR-CESM1-CAM5 and ACCESS3-1, over 10% (Figures S4–S6). In the northern areas, the impact of truncation for ill-behaved models is at most ~10% (Figures S7–S10).

Even in the polar areas, all features of the multimodel mean RH change are not sensitive to the excessively high modeled humidities. In particular, the large decline of RH over several high-latitude ocean areas is apparent both in the untruncated and truncated data. Over the Barents Sea, for instance, the maximum drying is about 14% in the truncated and 16% in untruncated data (Figure 5).

As an additional assignment, we calculated the RH responses from unmodified monthly data by solely considering those nine GCMs in which supersaturations were absent (Table 1; the MIROC models and FGOALS-s2 were also excluded due to the occurrence of supersaturation in daily output files). Focusing on those models totally eliminated the spurious negative RH response over East Antarctica (not shown). Nonetheless, such a small ensemble of GCMs may not be representative enough for elaborating RH projections for practical applications.

5. On the Physical Interpretation of the Findings

In the GCM output files, humidities exceeding 100% primarily occur in the areas and seasons with mean temperatures far below 0°C. In the model-produced time series, the degree of supersaturation correlates negatively with temperature fluctuations. Furthermore, the supersaturations ease by the end of the ongoing century, concurrently with projected warming. This indicates that the exceedingly high humidities are related to the occurrence of low air temperatures.

5.1. Supersaturations in the Real Atmosphere

In the real world, near-surface air supersaturations comparable to those occurring in the output files of several GCMs do not appear plausible. In southern polar areas, meteorological observations only reveal humidities slightly above 100% with respect to ice [*Andreas et al.*, 2002; *Genthon et al.*, 2010]. In the fringe areas of Antarctica, katabatic winds even act to engender quite low relative humidities, with time-mean values locally smaller than 40% [*Andersen et al.*, 2015].

Admittedly, in situ humidity measurements in below-freezing temperatures involve challenges. During potential supersaturation events, air humidity above the saturation vapor pressure with respect to ice (frost point) would tend to sublimate onto the device rather than getting measured by the sensing element [*Makkonen*, 1996].

On the other hand, in the free atmosphere a lack of freezing nuclei may allow substantial supersaturations. For example, by analyzing satellite measurements, *Gettelman et al.* [2006] reported humidities significantly above 100% with respect to ice at the 300 and 500 hPa levels over central Antarctica, particularly during autumn and winter.

5.2. Potential Causes of Supersaturations in Model Output

To survey potential causes behind the supersaturations apparent in the model output data, we also briefly explored modeled relative humidities in the free atmosphere represented at constant-pressure levels. This analysis included 14 models, excluding those for which pressure-level data were not available as well as parallel model versions from some modeling centers. For technical reasons, we limited this analysis to relatively short (typically 5 years) time series.

For 4 models out of the 14 ones analyzed within this subtask, the output data were completely free from supersaturations, both at the 2 m level and at isobaric levels: MRI-CGCM3, CNRM-CM5, IPSL-CM5A-LR, and CanESM2. In NCAR-CCSM4 and NorESM1-M, supersaturations were found in the near-surface layer but they were negligibly small in the lower tropospheric levels, at most ~ 0.1%. In INMCM4, GFDL-CM3, and GFDL-ESM2M, supersaturations were likewise far weaker (albeit not negligible) in the free atmosphere than near the surface. Conversely, prominent supersaturations occurred in both subdomains in MIROC5, HadGEM2-ES, ACCESS1-3, and in the daily data of MIROC-ESM. In CSIRO-Mk3-6-0, there were significant supersaturations in the free atmosphere but not in the near-surface layer. This suggests that, in this model, unphysically high humidities may have been truncated afterward from the near-surface data.

The above findings seem to indicate that the ultimate origin of the supersaturation issue diverges among the GCMs inspected. Evidently, in some models supersaturations originate from the core of the model algorithm, while in others they have been formed only in the stage of creating the surface air moisture fields. It is likely that in several models both factors play a role: some degree of supersaturation has developed within the dynamic calculations but the excessive relative humidities have further been amplified when building the surface air humidity fields. The divergent nature of the supersaturation issue is also reflected in the geographical distribution of supersaturation. For example, particularly in the Northern Hemisphere, in some models supersaturation mainly occurs over the Arctic Ocean, in others over continents (Figure 3).

Like the surface air fields, neither do the isobaric level fields represent the actual intrinsic model data but have been interpolated from the values given at model hybrid levels. A more comprehensive picture of the genuine modeled humidities would have been obtained by studying such vertically uninterpolated RH data. Unfortunately, original model-level data were only available from the IPSL models in which supersaturations do not occur (Table 1).

No harmonized documentation about the processing of surface air RH in individual models is available [*Byrne and O'Gorman*, 2016]. Therefore, to obtain a deeper insight into the reasons of the supersaturation problem, we contacted the modeling groups responsible for the GCMs analyzed in the present work. Feedback to our inquiry was received from more than a half of the groups consulted, even though several respondents regretted that their resources did not allow a comprehensive inspection of the problem. In the responses, potential explanations for the occurrence of supersaturations were roughly divided into three categories: the definition of RH with respect to ice rather than liquid water, contradictions in the determination of specific humidity and air temperature for the near-surface level, and the nonlinearity of saturated specific humidity as a function of temperature.

As stated in the previous subsection, in the free atmosphere moderate supersaturations with respect to ice are physically plausible due to the scarcity of icing nuclei. In the MIROC models, for instance, supersaturations with respect to ice (but not to liquid water) are additionally allowed at the lowermost model levels. The resulting high values of humidity are reflected in RH at the 2 m level. To give a theoretical upper limit, 100% RH with respect to supercooled liquid water would correspond to a 121% (147%) RH with respect to ice at the −20°C (−40°C) temperature [*Andersen et al.*, 2015, equation (1)]. In many models (e.g., MRI-CGCM3 and the GFDL models), RH is determined with respect to a blended ice-liquid water saturation pressure (rather than purely liquid water), and the resulting supersaturations with respect to ice would be more moderate. Presumably, this is at least a partial explanation for supersaturations in those models in which overly high RHs occur both in the near-surface data and higher aloft.

In many models, air temperature and specific humidity for the 2 m height are calculated independently by using the Monin-Obukhov similarity theory. Accordingly, the "interpolation" procedure is far more sophisticated than simple linear interpolation, for instance. If the values derived for near-surface specific humidity and air temperature are not mutually consistent, specific humidity may exceed the saturated specific humidity (that is determined by air temperature and pressure), leading to an apparent supersaturation. This potential explanation was mentioned in all of the three most comprehensive responses received to the query, i.e., in those from the centers hosting the NorESM, GFDL, and GISS models. This makes us to suspect that such an inconsistency may be quite a common source of supersaturations in the near-surface data. It is widely known that the treatment of extremely stably stratified boundary layers is challenging for atmospheric models; e.g., the Monin-Obukhov similarity theory applied generally in models does not work reliably [*Mahrt*, 2014]. According to the present analysis, spurious supersaturations tend to focus specifically on the polar areas of the winter hemisphere, i.e., on the areas where permanent surface inversions are most intense. Inconsistencies in boundary layer schemes may be responsible for RH >100% occurrence in those models in which supersaturations occur exclusive at 2 m or they are substantially stronger at 2 m than in the free atmosphere.

Moderate supersaturations may be caused by the nonlinear dependence of saturation-specific humidity on temperature. This possibility was mentioned, e.g., by the groups responsible for the INMCM4 and the GISS models. If air in the lowermost atmospheric layers is close to the saturation state and a strong temperature inversion prevails, supersaturation in the near-surface air may be generated by of the vertical interpolation scheme. To give a simple example, if air temperature at the ground level were −20°C and at the lowermost atmospheric model level −10°C, and RH at both levels 100%, a plain arithmetic averaging of specific humidity

and temperature between the levels would yield a RH of 110%. However, extremely high supersaturations are difficult to explain by this phenomenon alone.

The first of the explanations proposed above (RH calculated with respect to ice versus liquid water) is able to produce physically spurious humidities only in subzero temperatures. The two other phenomena, by contrast, may cause unrealistic relative humidities outside of the high-latitude areas as well, even though such artifacts do not become apparent as higher than 100% humidities in daily and monthly means.

In some models (e.g., BNU-ESM and BCC-CSM1-1) supersaturations do not occur since RH has deliberately been constrained to be $\leq$100% during the model run.

In several responses from the modeling groups it was emphasized that RH at 2 m is only an output product of the run that is not fed back into the model algorithm [cf. *Gleckler et al.*, 2008]. Hence, even the occurrence of pronounced supersaturation in the model output data (Table 1) does not generally invalidate model projections for other climate variables, e.g., temperature and precipitation.

6. Conclusions

In the archived output files of the majority of the CMIP5 GCMs inspected in this work, near-surface relative humidities above 100% with respect to ice are quite common in polar areas in winter. In conjunction with simulated future warming, the artificial supersaturations tend to weaken. This reduction of exceedances engenders a spurious negative trend in RH for high latitudes as a response to the RCP8.5 forcing. A truncation of the excessively high humidities in the model output before calculating the projections proved to eliminate this tendency, particularly over land areas. Conversely, over several high-latitude ocean areas, a substantial future decline in RH is preserved. Presumably, this oceanic trend is a true one, caused by the reduced static stability and enhanced vertical mixing induced by the retreat of sea ice.

Thereby, many previously published model-derived RH projections for polar continental areas should be regarded as suspicious. For example, the RH projection shown in Figure 12.21 of *IPCC* [2013] resembles that in our Figure 4a. In particular, a pronounced decline is apparent over East Antarctica, indicating that the projection has been founded on unmodified RH data.

It is evident that the truncation of excessively high humidities is not sufficient for eliminating all artifacts in the RH data. For example, during a day with the mean RH> 100%, RH may actually have stayed below 100% for a substantial time. Thereby, if the truncation of supersaturations were performed at an instantaneous level, the resulting daily mean RH would be below rather than equal to 100%. In addition, spuriously high humidities in polar areas may be a symptom of more widespread problems in the schemes used to calculate the near-surface RH. Accordingly, in the models exhibiting severe supersaturations at high latitudes, RH data might be questionable elsewhere as well. The RH data from those models should thus be taken with a caution globally, both when regarding recent past climate and projections for the future.

If unrealistic RH data are used as an input in climate change impact models, e.g., to calculate ice accumulation in tree crowns or moisture loads in buildings, the inferred consequences of climate change on the system may become severely distorted. In any case, it is highly recommendable to check the physical plausibility of the model-derived input data before using it for any application (or calculating multimodel means), but unfortunately this step is often neglected.

In the multimodel mean response, the impact of the truncation of spurious supersaturations proved to be minor outside of the polar areas. Nevertheless, in some individual GCMs (e.g., INMCM4, NCAR-CESM1-CAM5, and ACCESS1-3) the area affected by supersaturations was wider. In elaborating RH projections for northern boreal areas in winter, the projection should not be founded on any of these particular GCMs alone or on a limited ensemble of GCMs within which the weight of such ill-behaved models would be large.

Finally, we wholeheartedly recommend that all the institutes conducting CMIP6 GCM simulations should be informed about the supersaturation issue discussed in this work. Primarily, the procedures applied to producing near-surface RH data should be revised to avoid the occurrence of significant supersaturations. A straightforward truncation of higher than 100% humidities either during the model run or afterward before publishing the archived data does not solve the problem perfectly; rather, the algorithms used in calculating near-surface RH data should be reformulated to eliminate the fundamental causes of supersaturation. Even so, many modeling groups may not have sufficient resources to perform the required revisions within the

timetable allocated for the CMIP6 runs. It might therefore be appropriate to include RH extracted directly from the lowermost model hybrid level in the CMIP6 data archive, besides RH at the 2 m height; this field is not contaminated by the influence of vertical interpolations. To keep the sizes of data files reasonable and thus facilitate downloading the data, the lowermost-level RH fields should be provided as separate data files that do not contain RH data higher aloft in the atmosphere. The users could employ these data sets as a surrogate for near-surface air RH, e.g., by applying bias correction. In those models in which RH in subzero temperatures has been calculated with respect to a linear combination of the saturation pressures of ice and liquid water even at the lowest level, it would be preferable to directly publish this quantity rather than transforming it into RH with respect to ice. These measures might significantly mitigate the supersaturation problem in the output data of the next model generation and thus make the near-surface air humidity projections more reliable than those derived from the recent CMIP5 GCM ensemble.

Acknowledgments
This study has been performed under a contract (C3S_51_Lot4_FMI / DECM) for the Copernicus Climate Change Service. ECMWF implements this Service and the Copernicus Atmosphere Monitoring Service on behalf of the European Commission. Additional funding has been received from the Academy of Finland through the PLUMES project (decision 278067). The CMIP5 GCM data were downloaded from the Earth System Grid Federation (ESGF) data archive (http://esgf-node.llnl.gov/search/cmip5). All participating climate modeling groups are acknowledged for making their model output available through ESGF. Revisions induced by the comments presented by M. Juckes and an unknown reviewer have substantially deepened our insight into the subject. For information about near-surface RH calculations in the models, we are grateful for the following persons: A. Ackerman, I. Bethke, Y. Cheng, A. Del Genio, C. Fortelius, D. Ji, C.D. Jones, M. Kawamiya, K. Lo, Y. Lu, Ø. Seland, T. Toniazzo, E. Volodin, M. Watanabe, and S. Yukimoto, as well as for the GFDL Climate Model Info. As a part of this manuscript, an electronic supporting information file is available, containing figures displaying the influence of supersaturation on future projections for selected models. Also, maps of the ensemble-mean RH response using all 29 models are presented.

References

Andersen, D. T., C. P. McKay, and V. Lagun (2015), Climate conditions at perennially ice-covered Lake Untersee, East Antarctica, *J. Appl. Meteorol. Climatol.*, *54*, 1393–1412, doi:10.1175/JAMC-D-14-0251.1.

Andreas, E. L., P. S. Guest, P. O. G. Persson, C. W. Fairall, T. W. Horst, R. E. Moritz, and S. R. Semmer (2002), Near-surface water vapor over polar sea ice is always near ice saturation, *J. Geophys. Res.*, *107*(C10), 8033, doi:10.1029/2000JC000411.

Asseng, S., et al. (2015), Benchmark data set for wheat growth models: Field experiments and AgMIP multi-model simulations, *Open Data J. Agric. Res.*, *1*, 1–5, doi:10.17026/dans-zb6-6fvq.

Berg, A., et al. (2016), Land-atmosphere feedbacks amplify aridity increase over land under global warming, *Nat. Clim. Change*, *6*, 869–874, doi:10.1038/nclimate3029.

Byrne, M. P., and P. A. O'Gorman (2016), Understanding decreases in land relative humidity with global warming: Conceptual model and GCM simulations, *J. Clim.*, *29*, 9045–9061, doi:10.1175/JCLI-D-16-0351.1.

Ding, Y., and Y. Liu (2014), Analysis of long-term variations of fog and haze in China in recent 50 years and their relations with atmospheric humidity, *Sci. China Earth Sci.*, *57*, 36–46, doi:10.1007/s11430-013-4792-1.

Genthon, C., M. S. Town, D. Six, V. Favier, S. Argentini, and A. Pellegrini (2010), Meteorological atmospheric boundary layer measurements and ECMWF analyses during summer at Dome C, Antarctica, *J. Geophys. Res.*, *115*, D05104, doi:10.1029/2009JD012741.

Gettelman, A., V. P. Walden, L. M. Miloshevich, W. L. Roth, and B. Halter (2006), Relative humidity over Antarctica from radiosondes, satellites, and a general circulation model, *J. Geophys. Res.*, *111*, D09S13, doi:10.1029/2005JD006636.

Gleckler, P. J., K. E. Taylor, and C. Doutriaux (2008), Performance metrics for climate models, *J. Geophys. Res.*, *113*, D06104, doi:10.1029/2007JD008972.

Intergovernmental Panel on Climate Change (IPCC) (2013), *Climate Change 2013: The Physical Science Basis. Contribution of Working Group I to the Fifth Assessment Report of the Intergovernmental Panel on Climate Change*, edited by T. F. Stocker et al., 1535 pp., Cambridge Univ. Press, Cambridge, U. K.

Knutson, T. R., and J. J. Ploshay (2016), Detection of anthropogenic influence on a summertime heat stress index, *Clim. Change*, *138*, 25–39, doi:10.1007/s10584-016-1708-z.

Lahdensivu, J., H. Tietäväinen, and P. Pirinen (2011), Durability properties and deterioration of concrete facades made of insufficient frost resistant concrete, *Nord. Concr. Res.*, *44*, 175–188.

Lehtonen, I., K. Ruosteenoja, A. Venäläinen, and H. Gregow (2014), The projected 21st century forest-fire risk in Finland under different greenhouse gas scenarios, *Boreal Environ. Res.*, *19*, 127–139.

Lehtonen, I., M. Kämäräinen, H. Gregow, A. Venäläinen, and H. Peltola (2016), Heavy snow loads in Finnish forests respond regionally asymmetrically to projected climate change, *Nat. Hazards Earth Syst. Sci.*, *16*, 2259–2271, doi:10.5194/nhess-16-2259-2016.

Mahrt, L. (2014), Stably stratified atmospheric boundary layers, *Annu. Rev. Fluid Mech.*, *46*, 23–45, doi:10.1146/annurev-fluid-010313-141354.

Makkonen, L. (1996), Comments on "A method for rescaling humidity sensors at temperatures well below freezing", *J. Atmos. Oceanic Technol.*, *13*, 911–912, doi:10.1175/1520-0426(1996)013<0911:COMFRH>2.0.CO;2.

Makkonen, L., and B. Wichura (2010), Simulating wet snow loads on power line cables by a simple model, *Cold Reg. Sci. Technol.*, *61*, 73–81, doi:10.1016/j.coldregions.2010.01.008.

Parent, O., and A. Ilinca (2011), Anti-icing and de-icing techniques for wind turbines: Critical review, *Cold Reg. Sci. Technol.*, *65*, 88–96, doi:10.1016/j.coldregions.2010.01.005.

Ruosteenoja, K., and P. Räisänen (2013), Seasonal changes in solar radiation and relative humidity in Europe in response to global warming, *J. Clim.*, *26*, 2467–2481, doi:10.1175/JCLI-D-12-00007.1.

Ruosteenoja, K., T. Markkanen, A. Venäläinen, P. Räisänen, and H. Peltola (2017), Seasonal soil moisture and drought occurrence in Europe in CMIP5 projections for the 21st century, *Clim. Dyn.*, doi:10.1007/s00382-017-3671-4.

Seneviratne, S. I., T. Corti, E. L. Davin, M. Hirschi, E. B. Jaeger, I. Lehner, B. Orlowsky, and A. J. Teuling (2010), Investigating soil moisture-climate interactions in a changing climate: A review, *Earth Sci. Rev.*, *99*, 125–161, doi:10.1016/j.earscirev.2010.02.004.

Vajda, A., A. Venäläinen, I. Suomi, P. Junila, and H. M. Mäkelä (2014), Assessment of forest fire danger in a boreal forest environment: Description and evaluation of the operational system applied in Finland, *Meteorol. Appl.*, *21*, 879–887, doi:10.1002/met.1425.

van den Broeke, M., W. J. van de Berg, E. van Meijgaard, and C. Reijmer (2006), Identification of Antarctic ablation areas using a regional atmospheric climate model, *J. Geophys. Res.*, *111*, D18110, doi:10.1029/2006JD007127.

Viitanen, H., J. Vinha, K. Salminen, T. Ojanen, R. Peuhkuri, L. Paajanen, and K. Lähdesmäki (2010), Moisture and bio-deterioration risk of building materials and structures, *J. Building Phys.*, *33*, 201–224, doi:10.1177/1744259109343511.

Willett, K. M., and S. Sherwood (2012), Exceedance of heat index thresholds for 15 regions under a warming climate using the wet-bulb globe temperature, *Int. J. Climatol.*, *32*, 161–177, doi:10.1002/joc.2257.

Willett, K. M., R. J. H. Dunn, P. W. Thorne, S. Bell, M. de Podesta, D. E. Parker, P. D. Jones, and C. N. Williams Jr (2014), HadISDH land surface multi-variable humidity and temperature record for climate monitoring, *Climate of the Past*, *10*, 1983–2006, doi:10.5194/cp-10-1983-2014.